UC Davis
UC Davis Previously Published Works

Title

Ursodeoxycholic acid impairs liver-infiltrating T-cell chemotaxis through IFN-γ and CX3CL1 production in primary biliary cholangitis

Permalink

Journal

ISSN

Authors

Shimoyama, Shin
Kawata, Kazuhito
Ohta, Kazuyoshi
et al.

Publication Date

DOI

Peer reviewed

Check for updates

European Journal of **Immunology**

Immunomodulation and immune therapies

Clinical

Research Article

Ursodeoxycholic acid impairs liver-infiltrating T-cell chemotaxis through IFN-γ and CX3CL1 production in primary biliary cholangitis

Shin Shimoyama[1], Kazuhito Kawata[1] (ID) *, Kazuyoshi Ohta[1,2],*
Takeshi Chida[1,2], Tetsuro Suzuki[2], Koichi Tsuneyama[3], Shinji Shimoda[4],
Nobuhito Kurono[5], Patrick S.C. Leung[6], M. Eric Gershwin[6],
Takafumi Suda[1] and Yoshimasa Kobayashi[1]

[1] Hepatology Division, Department of Internal Medicine II, Hamamatsu University School of Medicine, Hamamatsu, Shizuoka, Japan

[2] Department of Virology and Parasitology, Hamamatsu University School of Medicine, Hamamatsu, Shizuoka, Japan

[3] Department of Pathology and Laboratory Medicine, Institute of Biomedical Sciences, Tokushima University Graduate School, Tokushima, Tokushima, Japan

[4] Department of Medicine and Biosystemic Science, Graduate School of Medical Sciences, Kyushu University, Fukuoka, Fukuoka, Japan

[5] Department of Chemistry, Hamamatsu University School of Medicine, Hamamatsu, Shizuoka, Japan

[6] Division of Rheumatology, Allergy and Clinical Immunology, University of California at Davis School of Medicine, Davis, CA, USA

Ursodeoxycholic acid (UDCA) is the primary treatment for primary biliary cholangitis (PBC), but its mechanism of action remains unclear. Studies suggest that UDCA enhances NF erythroid 2-related factor 2 (NFE2L2) expression and that the interaction between IFN-γ and C-X3-C motif chemokine ligand 1 (CX3CL1) facilitates biliary inflammation in PBC. Therefore, we examined the effects of UDCA on the expression of IFN-γ and CX3CL1 in in vitro and in vivo PBC models such as human liver tissue, a murine model, cell lines, and isolated human intrahepatic biliary epithelial cells (IHBECs). We observed a significant decrease in IFN-γ mRNA levels and positive correlations between IFN-γ and CX3CL1 mRNA levels post-UDCA treatment in PBC livers. NFE2L2-mediated transcriptional activation was significantly enhanced in UDCA-treated Jurkat cells. In 2-octynoic acid-immunized mice, IFN-γ production by liver-infiltrating T cells was dependent on NFE2L2 activation. IFN-γ significantly and dose-dependently induced CX3CL1 expression, which was significantly decreased in HuCC-T1 cells and IHBECs upon UDCA treatment. These results suggest that UDCA-induced suppression of IFN-γ and CX3CL1 production attenuates the chemotactic and adhesive abilities of liver-infiltrating T cells in PBC.

Keywords: CX3CL1 · IFN-γ · liver-infiltrating T cells · primary biliary cholangitis · ursodeoxycholic acid

🖥   Additional supporting information may be found online in the Supporting Information section at the end of the article.

Introduction

Primary biliary cholangitis (PBC) is a progressive autoimmune disease of the liver that exhibits Th1 cell cytokine predominance, which is characterized by portal tract lymphocytic infiltration and selective destruction of intrahepatic biliary epithelial cells (IHBECs) [1–6]. IFN-γ is known to stimulate the expression of C-X3-C motif chemokine ligand 1 (CX3CL1) [7], a CX3C chemokine. CX3CL1 and its receptor C-X3-C motif chemokine receptor 1 (CX3CR1) are recognized as key players in PBC-associated inflammation [8]. Th1 cells induce increased CX3CL1 expression in IHBECs, resulting in infiltration by CX3CR1-expressing mononuclear cells (MNCs) including CD4 and CD8 T cells [9, 10].

Ursodeoxycholic acid (UDCA) treatment improves both biochemical liver and liver pathology test results, and long-term treatment delays histological progression and improves survival rates in patients with early-stage PBC [11–14]. UDCA attenuates IHBEC damage through multiple mechanisms including bile acid pool modulation and choleretic, antiapoptotic, cytoprotective, antioxidant, and potentially immunomodulatory effects [15–21]. However, the molecular pathways underlying the immunomodulatory effects of UDCA on PBC have not been elucidated completely. However, it is also known that UDCA activates NF erythroid 2-related factor 2 (NFE2L2), a redox-sensitive transcription factor, inducing the coordinated expression of antioxidant genes [17, 22-24]. As NFE2L2 was recently demonstrated to modulate proinflammatory cytokine expression [25–31], in this study, we examined the effects of UDCA on IFN-γ production by liver-infiltrating T cells and CX3CL1 expression in IHBECs using in vitro and in vivo models of PBC.

Results

Comparison of hepatic proinflammatory cytokine and chemokine expression pre- and post-UDCA treatment

We examined pathological stages, cholangitis activities, and hepatitis activities upon UDCA treatment, and as expected, these activities improved (Fig. 1A). We then examined the levels of proinflammatory cytokines and chemokines in liver samples from patients with PBC pre- and post-UDCA treatment. Interestingly, the mRNA levels of *IFN-γ, IL4,* and *IL17* decreased significantly post-UDCA treatment; however, there were no significant changes in *CX3CL1* or *CX3CR1* mRNA levels (Fig. 1B). Although a significant association was not observed between *IFN-γ* and *CX3CL1* mRNA levels pre-UDCA treatment, there was a significant positive correlation post-UDCA treatment (Fig. 1C). Significant associations were also observed between *CX3CR1* and *CX3CL1* mRNA levels both pre- and post-UDCA treatment (Fig. 1D). Moreover, hepatic NFE2L2 protein levels increased significantly post-UDCA treatment in patients with PBC (Supporting Information Fig. S1).

### UDCA treatment enhances NFE2L2 activation in Jurkat cells

To assess whether UDCA treatment could enhance NFE2L2 activation in T cells, we evaluated *NFE2L2* transcriptional activity and mRNA levels of *NFE2L2* and NFE2L2-related antioxidant elements in Jurkat cells with and without UDCA treatment. The luciferase activity of the antioxidant responsive element (ARE) luciferase reporter vector was upregulated in UDCA-treated Jurkat cells (Fig. 2A). In addition, UDCA significantly increased the mRNA levels of *NFE2L2, heme oxygenase 1* (*HMOX1*), and *NAD(P)H quinone dehydrogenase 1* (*NQO1*) in Jurkat cells (Fig. 2B).

### Induction of autoimmune cholangitis in *Nfe2l2*-knockout mice

Based on the results in Jurkat cells, we next examined the effects of NFE2L2 activation on proinflammatory cytokine expression in liver-infiltrating T cells using a murine model of PBC. There was no significant hepatic pathology in $Nfe2l2^{+/+}$, $Nfe2l2^{+/-}$, or $Nfe2l2^{-/-}$ mice without 2-octynoic acid-BSA (2OA-BSA) immunization. After immunization with 2OA-BSA, histological examination of $Nfe2l2^{-/-}$ mice revealed significantly exacerbated portal inflammation, lobular inflammation, bile duct damage, and interface hepatitis (Fig. 3A and B). The absolute numbers of liver-infiltrating MNCs and CD8 T cells were significantly elevated in 2OA-BSA-immunized $Nfe2l2^{-/-}$ mice compared with that in 2OA-BSA-immunized $Nfe2l2^{+/+}$ mice (Fig. 3C and Supporting Information Fig. S2). IFN-γ concentrations in serum and liver protein extracts increased significantly in 2OA-BSA-immunized $Nfe2l2^{-/-}$ mice compared to those in 2OA-BSA-immunized $Nfe2l2^{+/+}$ mice (Fig. 4A and B). Significant increases in IFN-γ-producing CD4 T cells in the liver were noted in 2OA-BSA-immunized $Nfe2l2^{-/-}$ compared to those in 2OA-BSA-immunized $Nfe2l2^{+/+}$ mice. After 2OA-BSA immunization, IFN-γ-producing CD8 T cells in the liver were not elevated in $Nfe2l2^{-/-}$ mice compared to those in $Nfe2l2^{+/+}$ mice. Additionally, there were no significant changes in IL4- and IL17A-producing T cells in the livers of 2OA-BSA-immunized $Nfe2l2^{-/-}$ mice compared to those in 2OA-BSA-immunized $Nfe2l2^{+/+}$ mice (Fig. 4C).

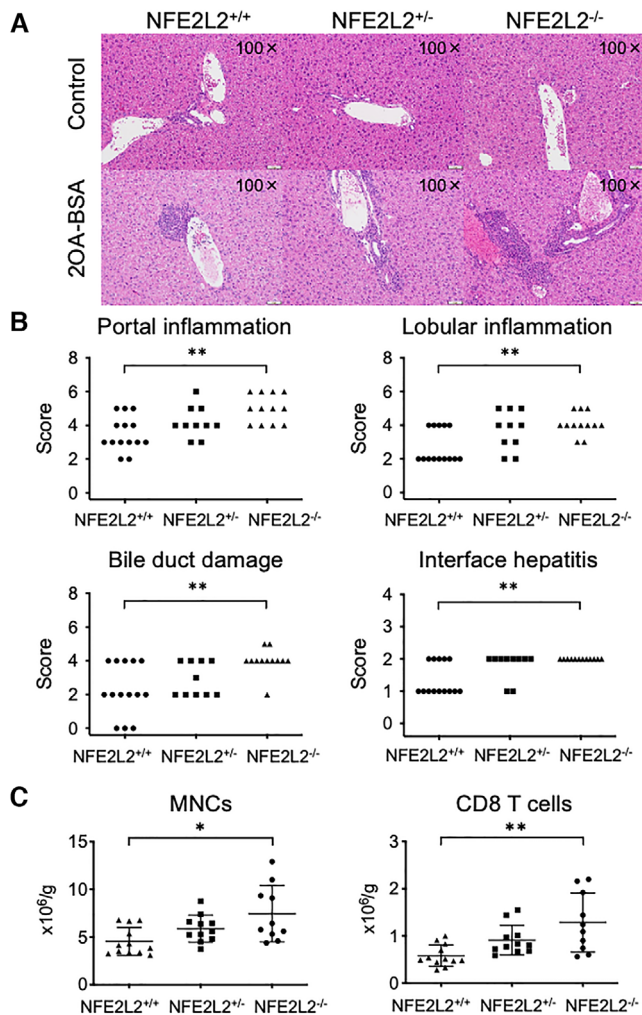### Induction of autoimmune cholangitis in NFE2L2-enhanced mice using sulforaphane

We next examined liver pathology and proinflammatory cytokine production by liver-infiltrating T cells in 2OA-BSA-immunized mice after treatment with sulforaphane (SFN), an NFE2L2 activator [32]. Given that treatment with UDCA has multiple effects, we used SFN instead of UDCA to focus exclusively on the effects of NFE2L2 activation on proinflammatory cytokine expression in liver-infiltrating T cells. *NFE2L2* mRNA levels were significantly increased in liver-infiltrating MNCs from 2OA-BSA-immunized
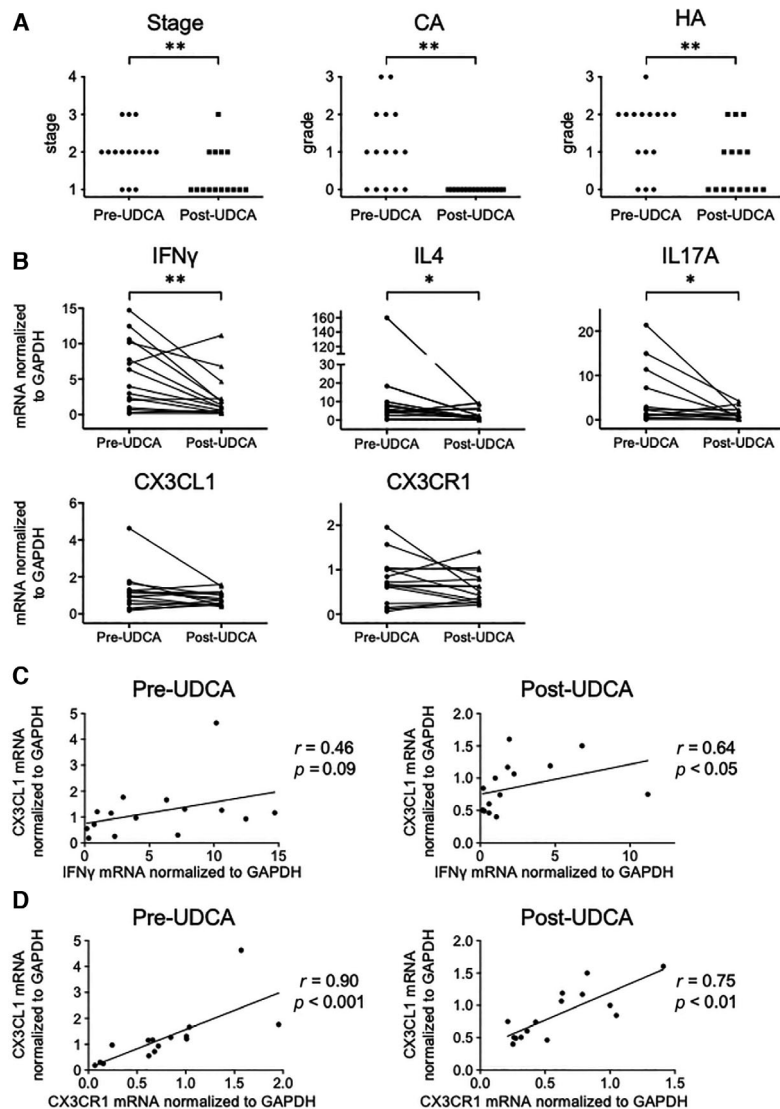
Figure 1. Pathology and proinflammatory cytokine and chemokine profiles of liver samples from 15 patients with primary biliary cholangitis (PBC) pre- and post-ursodeoxycholic acid (UDCA) treatment. (A) Histological comparison of tissues pre- and post-UDCA treatment using the Nakanuma histological staging and grading system. The staging score is the sum of the scores for fibrosis and bile duct loss. Cholangitis activities (CA) and hepatitis activities (HA) were graded from 0 to 3. (B) Comparison of *IFN-γ* (n = 15), *IL4* (n = 12), *IL17A* (n = 15), *CX3CL1* (n = 15), and *CX3CR1* (n = 15) mRNA levels normalized to GAPDH in pre- and post-UDCA treatment liver samples by quantitative PCR. (C) Correlation between IFN-γ and CX3CL1 mRNA levels in pre- and post-UDCA treatment liver samples. (D) Correlation between CX3CL1 and CX3CR1 mRNA levels in pre- and post-UDCA treatment liver samples. One experiment was performed, as described in the Methods section; *$p < 0.05$ and **$p < 0.01$, determined by Wilcoxon matched-pairs signed-rank test; correlation coefficients were calculated by linear correlation analysis.
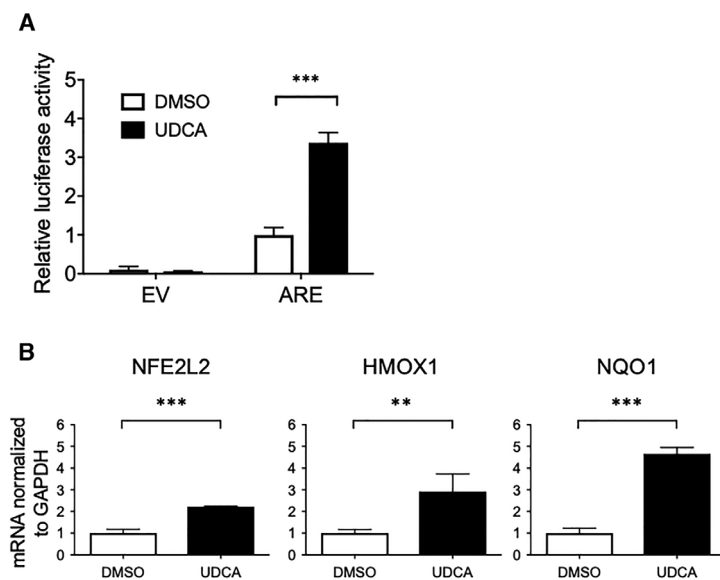
Figure 2. NFE2L2 activation in Jurkat cells with or without ursodeoxycholic acid (UDCA) treatment. (A) Luciferase activity in Jurkat cells with or without UDCA treatment. (B) *NFE2L2, HMOX1, and NQO1* mRNA levels normalized to GAPDH in Jurkat cells with or without UDCA treatment and measured by quantitative PCR. Values obtained using DMSO were set to 1. Three independent experiments with four samples per group in each experiment were performed. All data are presented as mean ± SD; **$p < 0.01$ and ***$p < 0.001$, determined by unpaired t-test. EV, empty vector.

A

Table 1. Absolute numbers of liver infiltrating cells ($\times 10^6$/g)

	DMSO (n=21)	SFN (n=18)	*p*-value
MNCs	5.11 ± 2.68	3.15 ± 1.10	<0.05
CD4 T cells	0.90 ± 0.45	0.59 ± 0.25	<0.05
CD8 T cells	0.71 ± 0.42	0.51 ± 0.23	N.S.
B cells	1.33 ± 0.50	0.95 ± 0.39	<0.05
NK cells	0.25 ± 0.18	0.13 ± 0.13	<0.01
NKT cells	0.32 ± 0.20	0.21 ± 0.13	N.S.

DMSO, dimethyl sulfoxide; SFN, sulforaphane; MNCs, mononuclear cells; NK, natural killer.

B

C

Figure 3. Autoimmune cholangitis in *Nfe2l2*-modified mice with 2OA-BSA immunization. (A) Representative H&E-stained liver sections of *Nfe2l2*$^{+/+}$ (n = 14), *Nfe2l2*$^{+/-}$ (n = 10), and *Nfe2l2*$^{-/-}$ (n = 12) mice with and without 2OA-BSA immunization from two independent experiments. Scale bar = 50 μm, Magnification 100 ×. (B) Scoring of portal inflammation, lobular inflammation, bile duct damage, and interface hepatitis after 2OA-BSA immunization from two independent experiments using *Nfe2l2*$^{+/+}$ (n = 14), *Nfe2l2*$^{+/-}$ (n = 10), and *Nfe2l2*$^{-/-}$ (n = 12) mice. (C) Flow cytometric analysis of lymphocytic liver infiltration in *Nfe2l2*-modified mice after 2OA-BSA immunization. The absolute numbers of mononuclear cells (MNCs) and CD8 T cells in the livers after 2OA-BSA immunization from two independent experiments using *Nfe2l2*$^{+/+}$ (n = 12), *Nfe2l2*$^{+/-}$ (n = 11), and *Nfe2l2*$^{-/-}$ (n = 10) mice were shown. These numbers are expressed as the number of cells per gram of liver tissue. All data are presented as mean ± SD; *p < 0.05 and **p < 0.01, determined by Kruskal–Wallis test followed by Dunn's multiple comparisons test.

mice treated with SFN compared to those in dimethyl sulfoxide (DMSO)-treated mice (Fig. 5A). Lobular inflammation and interface hepatitis in pathological examination were significantly ameliorated in 2OA-BSA-immunized mice treated with SFN compared with those in control mice (Fig. 5B). Furthermore, there were tendencies for amelioration in portal inflammation ($p = 0.07$) and bile duct damage ($p = 0.06$) (data not shown). The absolute numbers of liver-infiltrating MNCs, CD4 T cells, B cells, and NK cells

were significantly reduced in 2OA-BSA-immunized mice treated with SFN compared with those in control mice (Table 1). While SFN treatment did not result in significant changes in the frequencies of IL4- and IL17A-producing T cells, it significantly decreased the frequencies of IFN-γ-producing CD4 and CD8 T cells (Fig. 5C). Our data suggested that in 2OA-BSA-immunized mice, autoimmune cholangitis and IFN-γ production by liver-infiltrating T cells were dependent on NFE2L2 activation.

Attenuation of IFN-γ-induced CX3CL1 expression in cholangiocytes by UDCA

The results described above clarify the relationship between IFN-γ production and NFE2L2 activation in liver-infiltrating T cells of *Nfe2l2*-modified and NFE2L2-activated murine models of PBC. We next examined the effects of UDCA treatment on CX3CL1 production in IHBECs. *CX3CL1* mRNA levels in HuCC-T1 cells significantly decreased with decreasing IFN-γ concentrations, regardless of UDCA treatment. Furthermore, with 5000, 1000, and 500 IU/mL IFN-γ, *CX3CL1* mRNA expression was significantly suppressed by UDCA treatment (Fig. 6A). While total STAT1 expression remained unchanged, phosphorylated STAT1 (pSTAT1) levels after 1000 IU/mL IFN-γ stimulation were significantly repressed by UDCA treatment (Fig. 6B and Supporting Information Fig. S3). These results suggest that both decreased IFN-γ levels and UDCA treatment can attenuate CX3CL1 expression in HuCC-T1 cells. Similarly, *CX3CL1* mRNA levels were significantly decreased by UDCA treatment in human IHBECs (Fig. 6C). Moreover, CX3CL1 protein levels were reduced in the supernatants of UDCA-treated human IHBECs (Fig. 6D).

UDCA inhibits IFN-γ-receptor interactions on cholangiocytes

To clarify the mechanism underlying the inhibition of CX3CL1 production by UDCA, we examined whether UDCA inhibited IFN-γ binding to its receptors on HuCC-T1 cells. In HuCC-T1 cells stimulated with IFN-γ for 15 and 180 min, IFN-γ concentrations were significantly lower in UDCA-treated cells than those in DMSO-treated cells (Fig. 7), suggesting that UDCA interferes with IFN-γ-receptor interactions on HuCC-T1 cells. Taken together,
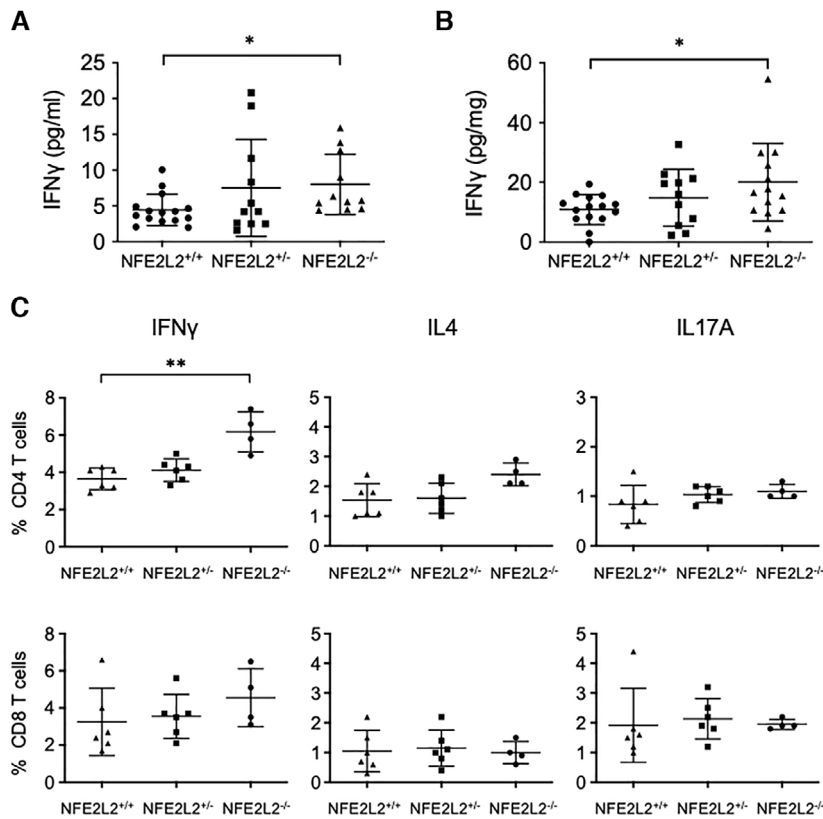
Figure 4. Proinflammatory cytokine profiles in *Nfe2l2*-modified mice with 2OA-BSA immunization. (A) Serum IFN-γ levels after 2OA-BSA immunization measured by the BD™ Cytometric Bead Array (CBA) and from two independent experiments using *Nfe2l2*$^{+/+}$ (n = 15), *Nfe2l2*$^{+/−}$ (n = 11), and *Nfe2l2*$^{−/−}$ (n = 11) mice. (B) IFN-γ concentrations in liver protein extracts after 2OA-BSA immunization measured by the BD™ CBA and from two independent experiments using *Nfe2l2*$^{+/+}$ (n = 15), *Nfe2l2*$^{+/−}$ (n = 11), and *Nfe2l2*$^{−/−}$ (n = 13). (C) The frequencies of IFN-γ-, IL4-, and IL17A-producing CD4 and CD8 T cells in the livers of *Nfe2l2*$^{+/+}$, *Nfe2l2*$^{+/−}$, and *Nfe2l2*$^{−/−}$ mice after 2OA-BSA immunization and analyzed by flow cytometry. The graphs were shown as one representative data from two independent experiments using *Nfe2l2*$^{+/+}$ (n = 13), *Nfe2l2*$^{+/−}$ (n = 11), and *Nfe2l2*$^{−/−}$ (n = 13) mice. All data are presented as mean ± SD; $^*p < 0.05$, $^{**}p < 0.01$, and $^{***}p < 0.001$, determined by Kruskal–Wallis test followed by Dunn's multiple comparisons test.
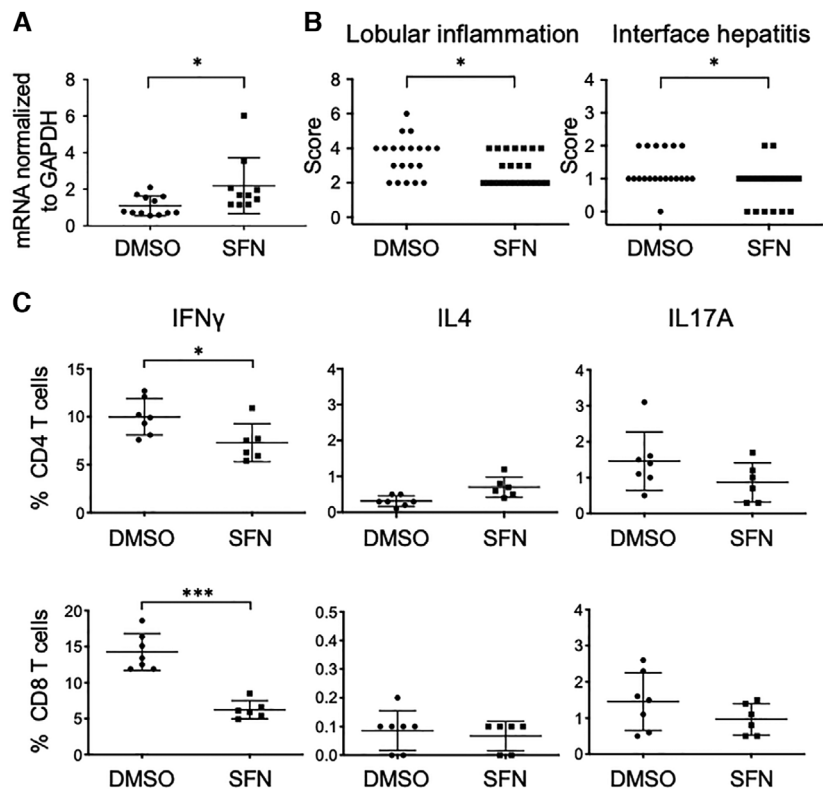

Figure 5. Autoimmune cholangitis and proinflammatory cytokine profiles in the livers of 2OA-BSA-immunized mice with NFE2L2 activation. (A) NFE2L2 mRNA levels normalized to GAPDH in liver-infiltrating mononuclear cells (MNCs) from 2OA-BSA-immunized mice treated with (n = 10) or without (n = 12) sulforaphane (SFN) in two independent experiments and measured by quantitative PCR. Values obtained from mice treated with dimethyl sulfoxide (DMSO) were set to 1. (B) Scoring of lobular inflammation and interface hepatitis in 2OA-BSA-immunized mice treated with (n = 24) or without (n = 20) SFN in three independent experiments. (C) The frequencies of IFN-γ-, IL4-, and IL17A-producing CD4 and CD8 T cells in the livers of 2OA-BSA-immunized mice treated with or without SFN and measured by flow cytometry. The graphs were shown as one representative data from two independent experiments using 2OA-BSA-immunized mice treated with (n = 9) or without (n = 11) SFN. All data are presented as mean ± SD; $^*p < 0.05$, $^{**}p < 0.01$, and $^{***}p < 0.001$, determined by Mann–Whitney U test.
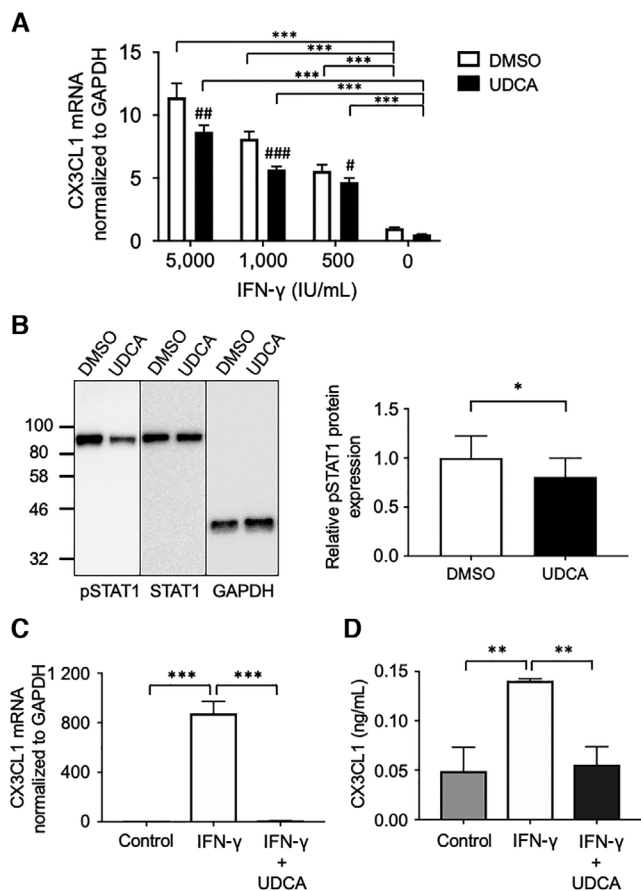
Figure 6. Ursodeoxycholic acid (UDCA) suppresses IFN-γ-induced CX3CL1 production in HuCC-T1 cells and intrahepatic biliary epithelial cells (IHBECs) from a patient with primary biliary cholangitis (PBC). CX3CL1 production was analyzed in HuCC-T1 cells preincubated with dimethyl sulfoxide (DMSO) or UDCA for 3 h before the 3 h treatment with IFN-γ. (A) CX3CL1 mRNA levels normalized to GAPDH at various IFN-γ concentrations and measured by quantitative PCR. Values obtained with DMSO alone were set to 1. Three independent experiments with four samples per group in each experiment were performed. $^*p < 0.05$, $^{**}p < 0.01$, and $^{***}p < 0.001$, determined by one-way ANOVA followed by Tukey's multiple comparisons test; $^\#p < 0.05$, $^{\#\#}p < 0.01$, and $^{\#\#\#}p < 0.001$, determined by unpaired t-test. (B) Representative immunoblot analyses of 1000 IU/mL IFN-γ-induced pSTAT1, STAT1, and GAPDH protein expressions are shown on the left panel. The quantification of pSTAT1 expression normalized to STAT1 is shown on the right panel. Three independent experiments with three or four samples per group in each experiment were performed. $^*p < 0.05$, determined by a paired t-test. (C) CX3CL1 mRNA levels normalized to GAPDH in control and IFN-γ-stimulated human IHBECs and measured by quantitative PCR. Values obtained from control cells were set to 1. One experiment with three samples per group was performed. (D) CX3CL1 protein levels in the supernatants of control and IFN-γ-stimulated human IHBECs measured by ELISA. One experiment with three samples per group was performed. $^{**}p < 0.01$ and $^{***}p < 0.001$, determined by one-way ANOVA followed by Tukey's multiple comparisons test. All data are presented as mean ± SD.

the data of this study indicate that UDCA both decreases IFN-γ production in liver-infiltrating T cells by activating NFE2L2 and inhibits IFN-γ from binding to its receptors on IHBECs, resulting in decreased CX3CL1 expression in these cells (Fig. 8).
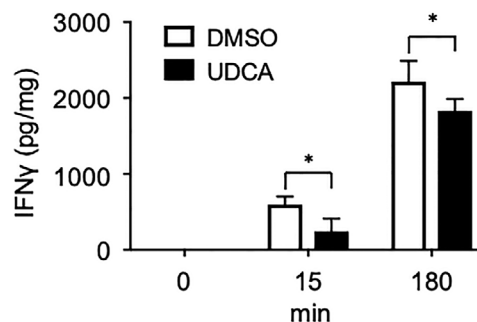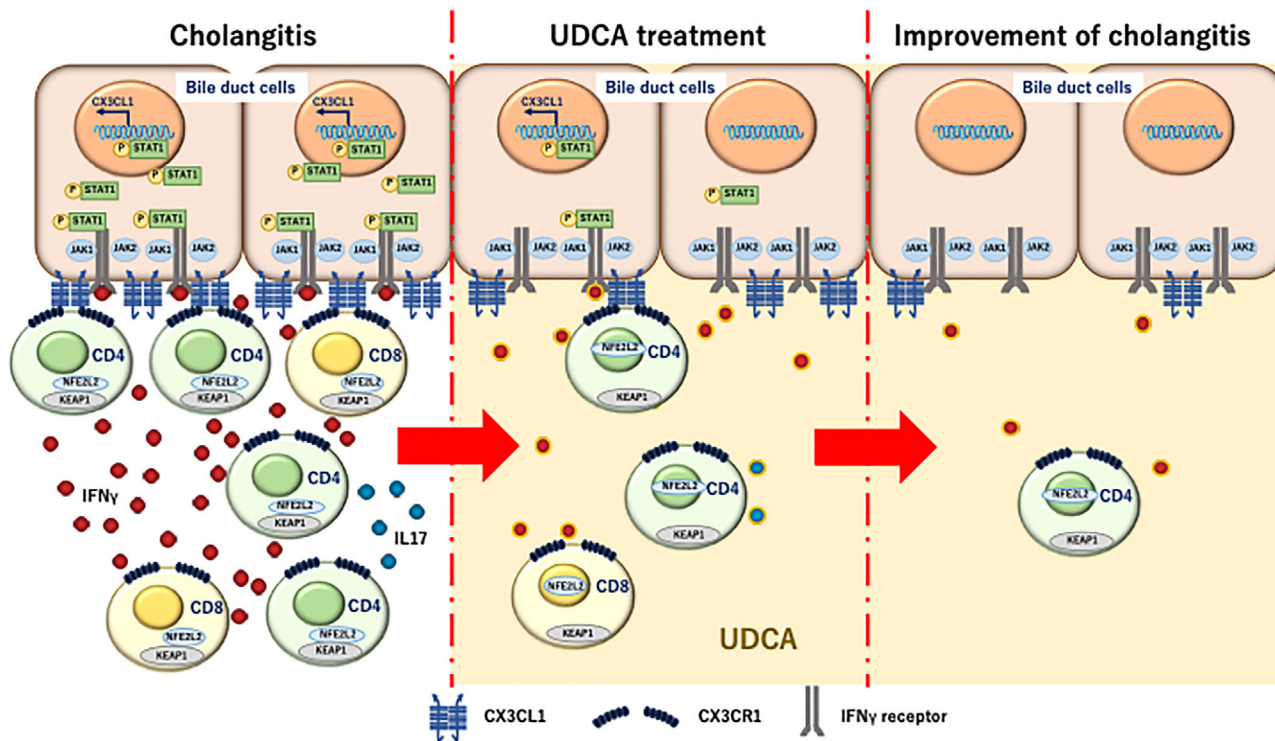

Figure 7. Ursodeoxycholic acid (UDCA) interferes with IFN-γ binding to its receptors on HuCC-T1 cells. IFN-γ concentrations were analyzed by the BD™ Cytometric Bead Array in HuCC-T1 cell lysates treated with 1000 IU/mL IFN-γ with 300 μM UDCA or dimethyl sulfoxide (DMSO) for 15 or 180 min. Three independent experiments with three or four samples per group in each experiment were performed. All data are presented as mean ± SD; $^*p < 0.05$, determined by unpaired t-test.

Discussion

UDCA is the first-line treatment for patients with PBC and is associated with improved survival without the need for liver transplantation [33,34]. However, the mechanism by which UDCA affects the immune response in autoimmune cholangitis is unclear. Previous studies have reported the activation of NFE2L2 signaling by UDCA in vivo and in vitro. UDCA increases NFE2L2 phosphorylation and promotes its translocation from the cytoplasm to the nucleus in Barrett's esophagus cells [22]. UDCA treatment also results in dose- and time-dependent increases in NFE2L2 expression in mouse vascular smooth muscle cells [23]. Furthermore, we previously demonstrated enhanced NFE2L2 activation and increased expression of NFE2L2-regulated antioxidant proteins in the livers of patients with PBC after UDCA treatment [17]. While NFE2L2 plays a crucial role in mitigating oxidative stress, its potential as a regulator of anti-inflammatory immune responses is a relatively recent notion. In the early phase of inflammation, NFE2L2 binds to AREs in the promoter regions of proinflammatory cytokine genes and inhibits their transcription in a ROS-independent manner. Additionally, in late-phase inflammation, NFE2L2 induces the transactivation of antioxidant enzymes and other cytoprotective genes in a ROS-dependent manner [26]. Recent studies have demonstrated that NFE2L2 activation might alter the Th1/Th2/Th17 cell balance [27-29, 35]. Here, we provide evidence that NFE2L2 affects immune regulation in autoimmune cholangitis. However, CX3CL1 mRNA levels did not differ in HuCC-T1 cells treated with or without UDCA, and there was no association between NFE2L2 activation and CX3CL1 levels in *Nfe2l2*-modified mice after 2OA-BSA immunization (data not shown), indicating that NFE2L2 might not be directly involved in CX3CL1 production in hepatic biliary cells. This prompted us to examine potential effects of UDCA on IFN-γ-receptor binding on IHBECs.

The major findings of this study are as follows. First, *IFN-γ* mRNA levels were significantly decreased and positively correlated with *CX3CL1* mRNA levels in livers with PBC post-UDCA

Figure 8. Model of the mechanism through which ursodeoxycholic acid (UDCA) attenuates the chemotactic and adhesive abilities of liver-infiltrating T cells in primary biliary cholangitis (PBC). Created by the authors themselves on PowerPoint. JAK1; Janus kinase 1; KEAP1; Kelch-like ECH-associated protein 1, pSTAT1; phosphorylated signal transducers and activators of transcription.

treatment. Second, UDCA upregulated the transcriptional activity of NFE2L2 in Jurkat cells. Third, IFN-γ production in liver-infiltrating CD4 T cells was dependent upon NFE2L2 activation in 2OA-BSA-immunized mice. This conclusion is also supported by the observation that increased NFE2L2 transcriptional activity in 2OA-BSA-immunized mice treated with SFN resulted in decreased liver IFN-γ-producing T cells. Last, IFN-γ-induced CX3CL1 expression and STAT1 phosphorylation in biliary epithelial cells were significantly reduced in a dose–dependent manner, and UDCA repressed IFN-γ-induced CX3CL1 expression in biliary epithelial cells by inhibiting IFN-γ binding to its receptors. Together, these results indicate that UDCA suppresses IFN-γ production by liver-infiltrating T cells and CX3CL1 expression in IHBECs, attenuating the chemotactic and adhesive abilities of liver-infiltrating MNCs, and improving cholangitis (Fig. 8).

We have systematically examined the interplay among IFN-γ, CX3CL1, and NFE2L2 upon UDCA treatment of PBC. Our study confirms that UDCA enhances NFE2L2 activation and increases the expression of NFE2L2 target genes in Jurkat cells. However, a previous study demonstrated that modulation of NFE2L2 activity had no effect on proinflammatory cytokine production in Jurkat cells [36]. Therefore, we studied the influence of NFE2L2 modulation on the production of inflammatory cytokines in liver-infiltrating T cells in mice with autoimmune cholangitis. We showed that IFN-γ production by liver-infiltrating T cells was dependent on NFE2L2 activation in 2OA-BSA-immunized mice. The immunoregulatory effects observed for UDCA are consis-

tent with previous observations. For example, the immunomodulatory effects of UDCA include reduced MHC class I and class II expression in hepatocytes and biliary epithelial cells [37,38] and normalization of NK cell activity through the inhibition of prostaglandin E2 production [39]. In addition, UDCA reduces IFN-γ production in liver lymphocytes via the glucocorticoid receptor [40]. Our results indicate that UDCA acts through dual pathways to suppress IFN-γ production in liver-infiltrating T cells, signaling through both the glucocorticoid receptor, as mentioned above, as well as through the NFE2L2 pathway.

Th1 and Th17 cell signaling pathways are both involved in the pathophysiology of PBC. While Th1 cytokines, especially IL-12 and IFN-γ, are associated with biliary inflammation and injury during the initiation process, after a shift in the Th1/Th17 balance, Th17 cytokines predominate, which correlates with the perpetuation of ongoing pathology in advanced-stage PBC [1]. CX3CL1, also known as fractalkine, is associated with the development of chronic nonsuppurative destructive cholangitis in PBC. Increasing CX3CL1 production in vascular endothelial cells via TLR3 and TLR4 stimulation and in IHBECs helps recruit CX3CR1-expressing MNCs, including CD4 and CD8 T cells, to these cells. The stimulation of Th1 cytokines from CX3CR1-expressing MNCs and TLR4 activation further augment the production of CX3CL1 from IHBECs, facilitating the development of chronic nonsuppurative destructive cholangitis [9,10]. Thus, Th1 cytokines and CX3CL1 signaling are potential molecular targets for PBC treatment. In this study, we observed decreased *IFN-γ* mRNA levels

but no changes in *CX3CL1* and *CX3CR1* mRNA levels in PBC liver samples after UDCA treatment. The mechanisms underlying alterations in CX3CL1 expression or the Th1/Th17 balance in patients with PBC during UDCA treatment have not yet been clarified. This study is the first assessment of changes in proinflammatory cytokines and CX3CL1 expression after UDCA treatment in PBC livers. Importantly, not only did we observe a decrease in IFN-γ mRNA expression, but also significant correlations between IFN-γ and CX3CL1 levels in the liver.

Our study has several limitations. First, neither were we able to compare the expression of NFE2L2 or proinflammatory cytokines in liver-infiltrating T cells nor chemokine expression in IHBECs in patients with PBC displaying adequate and inadequate responses to UDCA treatment. Second, while this study demonstrates for the first time that UDCA inhibits the binding of IFN-γ to its receptors, followed by the suppression of STAT1 phosphorylation and CX3CL1 production in IHBECs, the mechanism by which UDCA interferes with IFN-γ-receptor interactions remains unknown, and will require further study.

In conclusion, our data indicate that UDCA activates NFE2L2 in liver-infiltrating T cells by reducing IFN-γ production. The decreased IFN-γ level, combined with the inhibition of IFN-γ binding to receptors on IHBECs, results in reduced CX3CL1 expression in these cells. Together, the suppressed IFN-γ production in liver-infiltrating T cells and CX3CL1 production in IHBECs attenuates the chemotaxis of liver-infiltrating T cells and improves cholangitis.

Materials and methods

Human studies

Liver samples from sequential biopsies

Fifteen patients (3 males, 12 females; median age 60 $\pm$ 22 years) diagnosed with PBC in the Hepatology Division of the Department of Internal Medicine II at Hamamatsu University School of Medicine were included in this study. PBC diagnosis was based on the guidelines for the management of PBC proposed by the Intractable Hepatobiliary Disease Study Group, supported by the Ministry of Health, Labour and Welfare of Japan [41]. Patient selection was based on the availability of liver samples both pre- and post-UDCA treatment. All patients underwent their first liver biopsy before UDCA treatment, and their second biopsies were performed 2.7 $\pm$ 1.0 years after UDCA treatment (600 mg/day). All patients provided informed consent, and the study protocol was approved by the Ethics committee of Hamamatsu University School of Medicine and conformed to the ethical guidelines of the Declaration of Helsinki.

Liver tissues from sequential liver biopsies were fixed in formalin and embedded in paraffin, and subsequently stained with H&E. In addition, portions of the liver samples were immediately frozen in liquid nitrogen and stored at −80°C until use. Histolog-

ical staging of PBC was evaluated using the Nakanuma histologic staging and grading system [42,43] by a pathologist (M.G.) who was blinded to the clinical data.

Intrahepatic biliary epithelial cells

Human IHBECs were obtained from a patient with end-stage PBC who underwent orthotopic liver transplantation at Kyusyu University Hospital. Isolation of IHBECs was performed as previously described [44]. The purity of the isolated cells was >90%, based on immunohistochemical staining of cytokeratin 7 and cytokeratin 19 (Dako, Glostrup, Denmark). Cells were used after 4-6 passages. This protocol was approved by the Research Ethics Committee of Kyusyu University.

Jurkat cells and HuCC-T1 cells

Human T cell lymphoma Jurkat cells (RCB3052) and human intrahepatic cholangiocarcinoma HuCC-T1 cells (CRB0425) were purchased from RIKEN BRC through the National Bio-Resource Project of the MEXT/AMED (Japan) and the Health Science Research Resources Bank (Japan), respectively. The cells were grown in Roswell Park Memorial Institute (RPMI) 1640 Gluta-MAX medium (Thermo Fisher Scientific, Waltham, MA, USA) supplemented with 10% heat-inactivated fetal bovine serum (FBS; Thermo Fisher Scientific), 100 mg/mL streptomycin, and 100 U/mL penicillin (Thermo Fisher Scientific) at 37°C in a humidified incubator with 5% CO_2. For serum-reduced conditions (FBS $\leq$ 1%), 1 $\times$ Insulin Transferrin Selenium solution (ITS; Thermo Fisher Scientific) was added to the medium instead of FBS.

Plasmids and luciferase reporter assays

To construct the ARE luciferase reporter vector, oligonucleotides containing four ARE copies (TGACxxxGC) were inserted into the linearized pGL4.27 vector (Promega, Madison, WI, USA) using the In-Fusion HD Cloning Kit (Takara Bio, Tokyo, Japan). Jurkat cells (5.0 $\times$ 10^4) were seeded in 12-well plates and transiently transfected with the ARE luciferase reporter vector by electroporation using the Neon Transfection System (Thermo Fisher Scientific). Cells were incubated in serum-free RPMI 1640 medium with 300 μM UDCA or DMSO for 24 h. The activity of the ARE reporter vector was measured using the Dual-Luciferase Reporter Assay System (Promega) and an Infinite 200 Pro multimode reader (TECAN, Kanagawa, Japan). Firefly luciferase activity expressed from the ARE reporter vector was normalized to Renilla luciferase activity expressed from cotransfected pGL4.73.

Cell culture

HuCC-T1 cells were pretreated in serum-free medium supplemented with ITS with or without 300 μM UDCA for 3 h. Then, 0, 500, 1000, or 5000 IU/mL IFN-γ was added for an additional

15 or 180 min. Human IHBECs were pretreated in serum-free medium supplemented with ITS containing 300 μM UDCA for 3 h; 500 IU/mL IFN-γ was then added for an additional 3 h. The cells were harvested to extract proteins for IFN-γ concentration measurements and immunoblot analysis or RNA for RT-PCR, and the medium was collected to measure the CX3CL1 concentration.

IFN-γ and CX3CL1 measurements

IFN-γ concentrations in protein extracts were quantified using the BD^{TM} Cytometric Bead Array (CBA) Human Th1/Th2/Th17 Cytokine Kit (BD Biosciences, San Jose, CA, USA). Supernatant CX3CL1 concentrations were determined using a Quantikine enzyme-linked immunosorbent assay kit (R&D Systems, Minneapolis, MN, USA).

Immunoblot analysis

Frozen human liver tissues and HuCC-T1 cells were homogenized in protein extraction buffer (Santa Cruz Biotechnology, Dallas, TX, USA) containing a complete protease inhibitor cocktail (Roche Diagnostics, Mannheim, Germany). Lysates were diluted 1:1 with 2 × Laemmli sample buffer (Bio-Rad, Hercules, CA, USA) for SDS–PAGE on Mini-PROTEAN® TGX^{TM} Precast Protein Gels (Bio-Rad). The resolved proteins were electrophoretically transferred to polyvinylidene difluoride membranes using the iBlot Dry Blotting System (Thermo Fisher Scientific), which were blocked for 1 h at room temperature in TBST (20 mM Tris-HCl, pH 7.6, 137 mM NaCl, 0.5% Tween 20) containing 10% nonfat dry milk, and probed with the following primary antibodies: rabbit polyclonal anti-NFE2L2 (Santa Cruz Biotechnology; 1:100 dilution), rabbit polyclonal anti-GAPDH (Trevigen, Gaithersburg, MD, USA; 1:1000 dilution), mouse monoclonal anti-STAT1 (Cell Signaling Technology, Danvers, MA, USA; 1:1000 dilution), and rabbit monoclonal anti-pSTAT1 (Tyr701; Cell Signaling Technology, 1:1000 dilution). Bound primary antibodies were detected using the corresponding anti-rabbit or anti-mouse IgG HRP-conjugated secondary antibodies (Santa Cruz Biotechnology; 1:5000 dilution) and visualized by chemiluminescence using Amersham ECL Prime Western Blotting Detection Reagent (GE Healthcare Bio-Sciences, Uppsala, Sweden). Bands were quantified by densitometry using the software Image Lab version 5.2 (Bio-Rad) to obtain OD values, which were normalized to GAPDH.

RNA extraction and RT-PCR

Total RNA was extracted from Jurkat cells, HuCCT-1 cells, human IHBECs, and formalin-fixed, paraffin-embedded human liver tissues from sequential liver biopsies after deparaffinization using TRI Reagent (Molecular Research Center, OH) and reverse transcribed using the SuperScript VILO cDNA Synthesis Kit (Thermo Fisher Scientific). Aliquots of cDNA were subjected to 40 cycles of PCR amplification. Primer sequences are shown in Support-

ing information Table S1. Quantitative PCR was performed in the CFX Connect Real-Time System (Bio-Rad) using THUNDERBIRD SYBR qPCR mix (Toyobo, Osaka, Japan). Thermal cycling conditions were as follows: 1 min at 95°C, followed by 40 cycles at 95°C for 15 s and 60°C for 30 s. RNA expression data were normalized to GAPDH using the comparative threshold cycle method.

Murine studies

All animal experiments described below were performed with the approval of the Hamamatsu University School of Medicine Animal Care and Use Committee.

Induction of autoimmune cholangitis in *Nfe2l2*-knockout mice

Female WT C57BL/6JJmsSlc (B6) mice (*Nfe2l2$^{+/+}$*) were purchased from Japan SLC, Inc. (Hamamatsu, Japan). B6.129P2-Nfe2l2<tm1Mym>/MymRbrc (*Nfe2l2$^{-/-}$* and *Nfe2l2$^{+/-}$*) mice were purchased from RIKEN BRC through the National BioResource Project of the MEXT/AMED (Tsukuba, Japan) [45]. All mice were 6-10 weeks old and were housed in pathogen-free conditions. Autoimmune cholangitis was induced using 2OA, a synthetic chemical mimic of lipoic acid-lysine located within the inner domain of the E2 subunit of the pyruvate dehydrogenase complex, coupled with BSA (2OA-BSA) as previously described [46–48]. As control, another group of mice was injected in parallel with 100 μL of PBS.

Induction of autoimmune cholangitis in NFE2L2-activated mice

SFN, an NFE2L2 activator, was dissolved in DMSO. Autoimmune cholangitis was induced as described above, and the mice were intraperitoneally injected with either SFN (0.5 μg/g per body weight) or DMSO thrice weekly for 8 weeks after the initial 2OA-BSA immunization. At the end of the 8-week treatment, the mice were sacrificed, and their livers, spleens, and serum were immediately collected.

Murine liver analysis

Histological staging of murine cholangitis was evaluated using a defined scoring system by a blinded pathologist (K.T.). Portal inflammation and lobular inflammation were assigned severity and frequency scores. The severity scores were as follows: 0, none; 1, minimal; 2, mild; 3, moderate; and 4, severe. The frequency scores were as follows: 0, none; 1, 1-10%; 2, 11-20%; 3, 21-50%; and 4, >50%. Bile duct damage was also assigned severity and frequency scores. The severity scores were as follows: 0, none; 1, epithelial damage; 2, epithelial damage with nuclear changes; 3, chronic nonsuppurative destructive cholangitis; and 4, bile duct loss. The frequency scores were as described above.

Interface hepatitis was graded as follows: 0, none; 1, minimal; 2, mild; 3, moderate, and 4, severe.

For flow cytometry, liver-infiltrating MNCs were isolated using density gradient centrifugation with Histopaque-1077 (Density: 1.077; Sigma-Aldrich, St Louis, MO, USA). Then, isolated liver-infiltrating MNCs were incubated with purified anti-mouse CD16/32 antibody as Fc receptor blocking reagent (Biolegend, San Diego, CA, USA) and stained with a cocktail of PE/Cyanine7-conjugated anti-CD4 antibody, PerCP/Cyanine5.5-conjugated anti-CD19 antibody, APC/Cyanine7-conjugated anti-NK1.1 antibody, and APC-conjugated anti-T-cell receptor β antibody (Biolegend). A FACSAria (BD Biosciences) flow cytometer was used to acquire the data, which were analyzed with BD FACSDiva software version 6.1.3 (BD Biosciences).

To measure intracellular proinflammatory cytokines in liver-infiltrating T cells, MNCs were incubated in RPMI 1640 GlutaMAX medium with 100 μg/mL streptomycin, 100 U/mL penicillin, and 2 μL/mL Leukocyte Activation Cocktail, with BD GolgiPlug (BD Biosciences) for 4 h at 37°C in a humidified incubator with 5% CO_2. The cells were stained with PE/Cyanine7-conjugated anti-CD4 antibody, APC/Cyanine7-conjugated anti-NK1.1 antibody, and APC-conjugated anti-T-cell receptor β antibody, fixed and permeabilized with BD Cytofix/Cytoperm Solution (BD Biosciences), and subsequently stained with FITC-conjugated anti-IFN-γ antibody, PE-conjugated anti-IL4 antibody, and PerCP/Cyanine 5.5-conjugated anti-IL17A antibody (Biolegend). IgG isotype controls were used in parallel. Flow cytometry analyses were conducted accordingly to the guidelines used for immunological studies [49].

For measurements of IFN-γ levels in serum and liver protein extracts, IFN-γ concentrations were quantified using the BD™ CBA Mouse Th1/Th2/Th17 cytokine kit (BD Biosciences).

Finally, to quantify *NFE2L2* and *HMOX1* mRNA, total RNA was extracted from liver samples, and RT-PCR was performed using the primer sequences shown in Supporting information Table S1.

Statistical analysis

All statistical analyses were performed using GraphPad Prism (version 6.0; GraphPad Software, San Diego, CA, USA). Data are expressed as the mean $\pm$ SD and were evaluated with Wilcoxon matched-pairs signed rank tests, unpaired *t* tests, Mann-Whitney U tests, one-way ANOVA followed by Tukey's multiple comparisons tests, or Kruskal–Wallis tests followed by Dunn's multiple comparisons tests, as appropriate. Correlation coefficients were calculated by linear correlation analysis. $p < 0.05$ was considered statistically significant.

Author contributions: SS performed experiments and wrote the manuscript. KK designed experiments and helped write the manuscript. KO, TC, KT, SS, and NK performed experiments. TS, PSCL, and MEG assisted with experiments and writing the manuscript. TS and YK supervised the study.

Conflict of interest: The authors declare no commercial or financial conflict of interest.

Peer review: The peer review history for this article is available at https://publons.com/publon/10.1002/eji.202048589.

Data availability statement: The data that support the findings of this study are available from the corresponding author upon reasonable request.

References

1 **Yang, C.Y., Ma, X., Tsuneyama, K., Huang, S., Takahashi, T., Chalasani, N.P., Bowlus, C.L.**, et al., IL-12/Th1 and IL-23/Th17 biliary microenvironment in primary biliary cirrhosis: implications for therapy. *Hepatology* 2014. **59**: 1944–1953.

2 **Hirschfield, G.M., Liu, X., Xu, C., Lu, Y., Xie, G., Lu, Y., GU, X.**, et al., Primary biliary cirrhosis associated with HLA, IL12A, and IL12RB2 variants. *N. Engl. J. Med.* 2009. **360**: 2544–2555.

3 **Mells, G.F., Floyd, J.A., Morley, K.I., Cordell, H.J., Franklin, C.S., Shin, S.Y., Heneghan, M.A.**, et al., Genome-wide association study identifies 12 new susceptibility loci for primary biliary cirrhosis. *Nat. Genet.* 2011. **43**: 329–332.

4 **Nakamura, M., Nishida, N., Kawashima, M., Aiba, Y., Tanaka, A., Yasunami, M., Nakamura, H.**, et al., Genome-wide association study identifies TNFSF15 and POU2AF1 as susceptibility loci for primary biliary cirrhosis in the Japanese population. *Am. J. Hum. Genet.* 2012. **91**: 721–728.

5 **Sun, C., Xiao, X., Yan, L., Sheng, L., Wang, Q., Jiang, P., Lian, M**, et al., Histologically proven AMA positive primary biliary cholangitis but normal serum alkaline phosphatase: is alkaline phosphatase truly a surrogate marker? *J. Autoimmun.* 2019. **99**: 33–38.

6 **Tanaka, A., Leung, P.S.C.** and **Gershwin, M. E.**, Evolution of our understanding of PBC. *Best Pract. Res. Clin. Gastroenterol.* 2018. **34–35**: 3–9.

7 **Lee, M., Lee, Y., Song, J., Lee, J.** and **Chang, S. Y.**, Tissue-specific role of CX3CR1 expressing immune cells and their relationships with human disease. *Immune. Netw.* 2018. **18**: e5.

8 **Choi, J., Selmi, C., Leung, P.S., Kenny, T.P., Roskams, T.** and **Gershwin, M.E.**, Chemokine and chemokine receptors in autoimmunity: the case of primary biliary cholangitis. *Expert Rev. Clin. Immunol.* 2016. **12**: 661–672.

9 **Isse, K., Harada, K., Zen, Y., Kamihira, T., Shimoda, S., Harada, M.** and **Nakanuma, Y.**, Fractalkine and CX3CR1 are involved in the recruitment of intraepithelial lymphocytes of intrahepatic bile ducts. *Hepatology* 2005. **41**: 506–516.

10 **Shimoda, S., Harada, K., Niiro, H., Taketomi, A., Maehara, Y., Tsuneyama, K., Kikuchi, K**, et al., CX3CL1 (fractalkine): a signpost for biliary inflammation in primary biliary cirrhosis. *Hepatology* 2010. **51**: 567–575.

11 **Poupon, R E.**, **Lindor, K.D.**, **Pares, A.**, **Chazouilleres, O.**, **Poupon, R.** and **Heathcote, E.J.**, Combined analysis of the effect of treatment with ursodeoxycholic acid on histologic progression in primary biliary cirrhosis. *J. Hepatol.* 2003. **39**: 12–16.

12 **Corpechot, C.**, **Carrat, F.**, **Bahr, A.**, **Chretien, Y.**, **Poupon, R.E.** and **Poupon, R.**, The effect of ursodeoxycholic acid therapy on the natural course of primary biliary cirrhosis. *Gastroenterology* 2005. **128**: 297–303.

13 **Poupon, R.E.**, **Balkau, B.**, **Eschwege, E.** and **Poupon, R.**, A multicenter, controlled trial of ursodiol for the treatment of primary biliary cirrhosis. UDCA-PBC study group. *N. Engl. J. Med.* 1991. **324**: 1548–1554.

14 **Bahar, R.**, **Wong, K.A.**, **Liu, C.H.** and **Bowlus, C.L.**, Update on new drugs and those in development for the treatment of primary biliary cholangitis. *Gastroenterol. Hepatol. (N Y)* 2018. **14**: 154–163.

15 **Lazaridis, K.N.**, **Gores, G.J.** and **Lindor, K.D.**, Ursodeoxycholic acid 'mechanisms of action and clinical use in hepatobiliary disorders'. *J. Hepatol.* 2001. **35**: 134–146.

16 **Kawata, K.**, **Kobayashi, Y.**, **Gershwin, M.E.** and **Bowlus, C.L.**, The immunophysiology and apoptosis of biliary epithelial cells: primary biliary cirrhosis and primary sclerosing cholangitis. *Clin. Rev. Allergy Immunol.* 2012. **43**: 230–241.

17 **Kawata, K.**, **Kobayashi, Y.**, **Souda, K.**, **Kawamura, K.**, **Sumiyoshi, S.**, **Takahashi, Y.**, **Noritake H.**, et al., Enhanced hepatic Nrf2 activation after ursodeoxycholic acid treatment in patients with primary biliary cirrhosis. *Antioxid. Redox Signal.* 2010. **13**: 259–268.

18 **Tanaka, A.**, Emerging novel treatments for autoimmune liver diseases. *Hepatol. Res.* 2019. **49**: 489–499.

19 **Amaral, J.D.**, **Castro, R.E.**, **Sola, S.**, **Steer, C.J.** and **Rodrigues, C.M.**, p53 is a key molecular target of ursodeoxycholic acid in regulating apoptosis. *J. Biol. Chem.* 2007. **c282**: 34250–34259.

20 **Chen, W.**, **Wei, Y.**, **Xiong, A.**, **Li, Y.**, **Guan, H.**, **Wang, Q.**, **Miao, Q.**, et al., Comprehensive analysis of serum and fecal bile acid profiles and interaction with gut microbiota in primary biliary cholangitis. *Clin. Rev. Allergy Immunol.* 2020. **58**: 25–38.

21 **Tang, R.**, **Wei, Y.**, **Li, Y.**, **Chen, W.**, **Chen, H.**, **Wang, Q.**, **Yang, F.**, et al., Gut microbial profile is altered in primary biliary cholangitis and partially restored after UDCA therapy. *Gut* 2018. **67**: 534–541.

22 **Peng, S.**, **Huo, X.**, **Rezaei, D.**, **Zhang, Q.**, **Zhang, X.**, **Yu, C.**, **Asanuma, K.**, et al., In Barrett's esophagus patients and Barrett's cell lines, ursodeoxycholic acid increases antioxidant expression and prevents DNA damage by bile acids. *Am. J. Physiol. Gastrointest. Liver Physiol.* 2014. **307**: G129–G139.

23 **Liu, W.**, **Wang, B.**, **Wang, T.**, **Liu, X.**, **He, X.**, **Liu, Y.**, **Li, Z.**, et al., Ursodeoxycholic acid attenuates acute aortic dissection formation in angiotensin II-infused apolipoprotein E-deficient mice associated with reduced ROS and increased Nrf2 levels. *Cell Physiol. Biochem.* 2016. **38**: 1391–1405.

24 **Okada, K.**, **Shoda, J.**, **Taguchi, K.**, **Maher, J.M.**, **Ishizaki, K.**, **Inoue, Y.**, **Ohtsuki, M.**, et al., Ursodeoxycholic acid stimulates Nrf2-mediated hepatocellular transport, detoxification, and antioxidative stress systems in mice. *Am. J. Physiol. Gastrointest. Liver Physiol.* 2008. **295**: G735–G747.

25 **Kobayashi, E.H.**, **Suzuki, T.**, **Funayama, R.**, **Nagashima, T.**, **Hayashi, M.**, **Sekine, H.**, **Tanaka, N.**, et al., Nrf2 suppresses macrophage inflammatory response by blocking proinflammatory cytokine transcription. *Nat. Commun.* 2016. **7**: 11624.

26 **Keleku-Lukwete, N.**, **Suzuki, M.** and **Yamamoto, M.**, An overview of the advantages of KEAP1-NRF2 system activation during inflammatory disease treatment. *Antioxid. Redox Signal.* 2018. **29**: 1746–1755.

27 **Suzuki, T.**, **Murakami, S.**, **Biswal, S.S.**, **Sakaguchi, S.**, **Harigae, H.**, **Yamamoto, M.** and **Motohashi, H.**, Systemic activation of NRF2 alleviates lethal autoimmune inflammation in scurfy mice. *Mol. Cell. Biol.* 2017. **37**: e00063–17.

28 **Macoch, M.**, **Morzadec, C.**, **Genard, R.**, **Pallardy, M.**, **Kerdine-Romer, S.**, **Fardel, O.** and **Vernhet, L.**, Nrf2-dependent repression of interleukin-12 expression in human dendritic cells exposed to inorganic arsenic. *Free Radic. Biol. Med.* 2015. **88**: 381–390.

29 **Li, B.**, **Cui, W.**, **Liu, J.**, **Li, R.**, **Liu, Q.**, **Xie, X.H.**, **Ge, X.L.**, et al., Sulforaphane ameliorates the development of experimental autoimmune encephalomyelitis by antagonizing oxidative stress and Th17-related inflammation in mice. *Exp. Neurol.* 2013. **250**: 239–249.

30 **Nagashima, R.**, **Kosai, H.**, **Masuo, M.**, **Izumiyama, K.**, **Noshikawaji, T.**, **Morimoto, M.**, **Kumaki, S.**, et al., Nrf2 suppresses allergic lung inflammation by attenuating the type 2 innate lymphoid cell response. *J. Immunol.* 2019. **202**: 1331–1339.

31 **Subedi, L.**, **Lee, J.H.**, **Yumnam, S.**, **Ji, E.** and **Kim, S.Y.**, Anti-inflammatory effect of sulforaphane on LPS-activated microglia potentially through JNK/AP-1/NF-kappaB inhibition and Nrf2/HO-1 activation. *Cells* 2019. **8**: 194.

32 **Houghton, C.A.**, **Fassett, R.G.** and **Coombes, J.S.**, Sulforaphane: translational research from laboratory bench to clinic. *Nutr. Rev.* 2013. **71**: 709–726.

33 **Goel, A.** and **Kim, W.R.**, Natural history of primary biliary cholangitis in the ursodeoxycholic acid era: role of scoring systems. *Clin. Liver Dis.* 2018. **22**: 563–578.

34 **Lindor, K.D.**, **Bowlus, C.L.**, **Boyer, J.**, **Levy, C.** and **Mayo, M.**, Primary biliary cholangitis: 2018 practice guidance from the American Association for the Study of Liver Diseases. *Hepatology* 2019. **69**: 394–419.

35 **Rockwell, C.E.**, **Zhang, M.**, **Fields, P.E.** and **Klaassen, C.D.**, Th2 skewing by activation of Nrf2 in CD4(+) T cells. *J. Immunol.* 2012. **188**: 1630–1637.

36 **Morzadec, C.**, **Macoch, M.**, **Sparfel, L.**, **Kerdine-Romer, S.**, **Fardel, O.** and **Vernhet, L.**, Nrf2 expression and activity in human T lymphocytes: stimulation by T cell receptor activation and priming by inorganic arsenic and tert-butylhydroquinone. *Free Radic. Biol. Med.* 2014. **71**: 133–145.

37 **Calmus, Y.**, **Gane, P.**, **Rouger, P.** and **Poupon, R.**, Hepatic expression of class I and class II major histocompatibility complex molecules in primary biliary cirrhosis: effect of ursodeoxycholic acid. *Hepatology* 1990. **11**: 12–15.

38 **Terasaki, S.**, **Nakanuma, Y.**, **Ogino, H.**, **Unoura, M.** and **Kobayashi, K.**, Hepatocellular and biliary expression of HLA antigens in primary biliary cirrhosis before and after ursodeoxycholic acid therapy. *Am. J. Gastroenterol.* 1991. **86**: 1194–1199.

39 **Nishigaki, Y.**, **Ohnishi, H.**, **Moriwaki, H.** and **Muto, Y.**, Ursodeoxycholic acid corrects defective natural killer activity by inhibiting prostaglandin E2 production in primary biliary cirrhosis. *Dig. Dis. Sci.* 1996. **41**: 1487–1493.

40 **Takigawa, T.**, **Miyazaki, H.**, **Kinoshita, M.**, **Kawarabayashi, N.**, **Nishiyama, K.**, **Hatsuse, K.**, **Ono, S.**, et al., Glucocorticoid receptor-dependent immunomodulatory effect of ursodeoxycholic acid on liver lymphocytes in mice. *Am. J. Physiol. Gastrointest. Liver Physiol.* 2013. **305**: G427–G438.

41 Working Subgroup for Clinical Practice Guidelines for Primary Biliary C. Guidelines for the management of primary biliary cirrhosis: the Intractable Hepatobiliary Disease Study Group supported by the Ministry of Health, Labour and Welfare of Japan. *Hepatol. Res.* 2014. **44**: 71–90.

42 **Hiramatsu, K.**, **Aoyama, H.**, **Zen, Y.**, **Aishima, S.**, **Kitagawa, S.** and **Nakanuma, Y.**, Proposal of a new staging and grading system of the liver for primary biliary cirrhosis. *Histopathology* 2006. **49**: 466–478.

43 **Nakanuma, Y.**, **Zen, Y.**, **Harada, K.**, **Sasaki, M.**, **Nonomura, A.**, **Uehara, T.**, **Sano, K.**, et al., Application of a new histological staging and grading system for primary biliary cirrhosis to liver biopsy specimens: interobserver agreement. *Pathol. Int.* 2010. **60**: 167–174.

44 **Shimoda, S.**, **Hisamoto, S.**, **Harada, K.**, **Iwasaka, S.**, **Chong, Y.**, **Nakamura, M.**, **Bekki, Y.**, et al., Natural killer cells regulate T cell immune responses in primary biliary cirrhosis. *Hepatology* 2015. **62**: 1817–1827.

45 Itoh, K., Chiba, T., Takahashi, S., Ishii, T., Igarashi, K., Katoh, Y., Oyake, T., et al., An Nrf2/small Maf heterodimer mediates the induction of phase II detoxifying enzyme genes through antioxidant response elements. *Biochem. Biophys. Res. Commun.* 1997. **236**: 313–322.

46 Kawata, K., Tsuda, M., Yang, G. X., Zhang, W., Tanaka, H., Tsuneyama, K., Leung, P., et al., Identification of potential cytokine pathways for therapeutic intervention in murine primary biliary cirrhosis. *PLoS One* 2013. **8**: e74225.

47 Wakabayashi, K., Lian, Z.X., Leung, P.S., Moritoki, Y., Tsuneyama, K., Kurth, M.J., Lam, K.S., et al., Loss of tolerance in C57BL/6 mice to the autoantigen E2 subunit of pyruvate dehydrogenase by a xenobiotic with ensuing biliary ductular disease. *Hepatology* 2008. **48**: 531–540.

48 Dhirapong, A., Yang, G.X., Nadler, S., Zhang, W., Tsuneyama, K., Leung, P., Knechtle, S., et al., Therapeutic effect of cytotoxic T lymphocyte antigen 4/immunoglobulin on a murine model of primary biliary cirrhosis. *Hepatology* 2013. **57**: 708–715.

49 Cossarizza, A., Chang, H. D., Radbruch, A., Acs, A., Adam, D., AdamKlages, S., Agace, W. W. et al., Guidelines for the use of flow cytometry and cell sorting in immunological studies (second edition). *Eur. J. Immunol.* 2019. **49**: 1457–1973.

Full correspondence: Dr. Kazuhito Kawata, Department of Internal Medicine II, Hamamatsu University School of Medicine, 1-20-1 Handayama, Higashiku, Hamamatsu, Shizuoka 431–3192, Japan
e-mail: kawata@hama-med.ac.jp